The International Journal of Advanced Manufacturing Technology (2020) 110:1095–1111
https://doi.org/10.1007/s00170-020-05888-5

ORIGINAL ARTICLE

Compatibilization of PA6/ABS blend by SEBS-g-MA: morphological, mechanical, thermal, and rheological properties

H. Essabir[1,2] · F. Z. El Mechtali[3] · S. Nekhlaoui[3] · M. Raji[1] · M. O. Bensalah[3] · D. Rodrigue[4] · R. Bouhfid[1] · A. Qaiss[1]

Received: 14 December 2019 / Accepted: 5 August 2020 / Published online: 20 August 2020

Abstract

Blends polyamide 6 (PA6) and acrylonitrile-butadiene-styrene (ABS) were compatibilized with a styrene–(ethylene–butene)–styrene triblock copolymer grafted with maleic anhydride (SEBS-g-MA). In particular, the effects of ABS (0–100 wt%) and compatibilizer (0, 8, and 16 wt%) content were studied. The blends were first prepared by twin-screw extrusion, and different specimens were prepared by injection molding. From the samples produced, the effects of blend composition on morphological, mechanical, rheological, and thermal properties are reported. The structural analysis confirmed that the original blend is immiscible but showed some compatibilization when in the presence of SEBS-g-MA. Incorporation of the compatibilizer and ABS showed negligible effect on the melting behavior of PA6. The compatibilized blends showed higher tensile strength compared with uncompatibilized ones. However, Young's modulus decreased with increasing compatibilizer content. The mechanical results were confirmed by rheological measurements in terms of interaction between each components in the blend.

Keywords Polyamide 6 · Acrylonitrile–butadiene–styrene · Blend; Compatibilization · Morphology

1 Introduction

Still today, polymer blending is an important and active area in the field of material processing specially to improve the general properties of neat polymers [1, 2]. Blending of polymers gained credibility as a simple approach to create novel materials without the cost associated with synthesis of new molecules [3]. Polymer blends were mainly developed to meet technical requirements that neat resins were unable to achieve [4]. Also, blending existing polymers is less expensive than developing a new polymer [5]. However, most polymer blends are immiscible systems and this has substantial influence on their properties and performances since they are mainly determined by their morphology, i.e., the distribution of each components in terms of size and form [6, 7]. Phase separation in the blends, due to immiscibility, leads to low mechanical properties because of poor interactions between each phase. These unfavorable interactions lead to significant interfacial tension in the melt state and low interfacial adhesion in the solid state leading to a multiphase morphology [8, 9]. Nevertheless, the properties of polymer blends are not only a function of interfacial interaction between the components but also depend on the dispersed phase size and blend composition (general blend morphology), which can be controlled by processing conditions. Usually, two types of morphologies are formed: the sea-island morphology and the co-continuous morphology [10, 11] . In contrast, other classes of polymers blend are not inert. They may interact strongly with the environment and adopt special functions. Examples include specific interactions with molecules and ions exploited in separation and purification techniques; electrical and optical properties used in polymer solar cells, organic light emitters, and optical elements; and properties relevant for solar cell application [12–14].

✉ H. Essabir
h.essabir@uiz.ac.ma

✉ A. Qaiss
a.qaiss@mascir.com

[1] Moroccan Foundation for Advanced Science, Innovation and Research (MAScIR), Institute of Nanomaterials and Nanotechnology (NANOTECH), Composites and Nanocomposites Center, Rabat, Morocco

[2] Mechanic, Materials and composites (MMC), Laboratory of Energy Engineering, Materials and Systems, National School of Applied Sciences of Agadir, Ibn Zohr University, Agadir, Morocco

[3] Faculty of Science, Laboratory of Mechanic and Materials (LMM), Mohammed V-Agdal University, Rabat, Morocco

[4] Department of chemical engineering and CERMA, Université Laval, Quebec G1V0A6, Canada

Polymer blends based on polyamide 6 (PA6) have gained large attention in industrial applications because they combine excellent mechanical properties and easy processability [15, 16]. PA6 has attracted a particular attraction because of a good balance between high strength/stiffness, low friction, and excellent chemical/wear resistance. These properties led to a wide range of applications like automotive, electrical, and mechanical/structural [17, 18] . However, PA6 has some disadvantages such as high mold shrinkage and low-dimensional stability due to its rapid crystallization and high moisture sensitivity (hygroscopic nature). On the other hand, acrylonitrile–butadiene–styrene (ABS) terpolymer is better compared with PA6 in terms of low mold shrinkage, ease of processing, low water absorption, and high impact strength. It is also more interesting from an economic point of view since ABS is less expensive than PA6 [19]. Recently, several investigations were devoted to PA6/ABS blends [19, 20]. If optimized, blending PA6 with ABS could be an interesting route to achieve new materials with promising property combinations. Nevertheless, it was reported that blends of PA6 and ABS are immiscible and exhibit low impact toughness because butadiene particles formed during melt blending are relatively large. Moreover, ABS consist of butadiene rubber dispersed in a styrene–acrylonitrile copolymer matrix. The rubber phase can improve the low-temperature toughness of PA6, while the styrene–acrylonitrile copolymer phase provides stiffness [21]. Therefore, PA6/ABS blends were found to have high thermal stability and high mechanical properties [22]. Nevertheless, when good chemical resistance and high dimensional stability is required, PA6, with its highly polar functional group, is not miscible with ABS, so their blends exhibit a limitation in final properties under specific conditions leading to phase separation. One effective way to overcome the limitation of immiscibility is the introduction of a third component which can act as an interfacial agent to reduce the interfacial tension and promote adhesion at the interface[23].

In the present work, ABS that is blended with PA6 using a twin-screw extruder and styrene–(ethylene–butene)–styrene triblock copolymer grafted with maleic anhydride (SEBS-g-MA) is used as a compatibilizer to improve interfacial adhesion. The idea is to improve interfacial adhesion and ductility decreased of the polymer after using a rigid part (ABS). For these reasons, the modification is due by grafting a functional group such as maleic anhydride to ensure a good interfacial adhesion (coupling agent behavior) where a MA function on a styrene–(ethylene–butene)–styrene triblock copolymer was grafted as a rubber part to confer to material a ductile behavior [24, 25]. The samples were then injection molded to perform a complete morphological, thermal, mechanical, and rheological characterization of the blends to investigate the effect of ABS and SEBS-g-MA content. In this work, besides the structural, morphological, and thermomechanical characterization, the rheological properties were investigated in the solid state (applications) and in the molten state to simulate the material behavior under processing (viscosity). On the other hand, the modeling approach via standard models such as Voigt, Reuss, Hirsch, and Tsai-Pagano was used to characterize the adhesion level at the interface with addition of SEBS-g-MA.

2 Materials and methods

2.1 Materials

Polyamide 6 (PA6) Ultramid O was obtained from BASF (density = 1.13 g/cm^3 and melting temperature = 220 °C), while acrylonitrile–butadiene–styrene (ABS) terpolymer was purchased from SODEVIC (density = 1.04 g/cm^3 and melting temperature = 220°C). A triblock copolymer styrene–(ethylene–butene)–styrene grafted with 1.4 to 2 wt % maleic anhydrides (SEBS-g-MA) (Kraton FG-1901X) supplied by Shell was used as coupling agent (Table 1).

2.2 Experimental procedure

Three compatibilizer (SEBS-g-MA) contents were used (0, 8, and 16 wt%) with different ABS contents (5, 15, 25, 35, 40, 45, 50, 55, 60, 65, 75, 85, 95, 100 wt%) to prepare binary (PA6/ABS) and ternary (PA6-SEBS-g-MA-ABS) blends (Table 2) . The compounds were prepared on a Leistritz ZSE-18 twin-screw extruder operating at a screw speed of 125 rpm (L/D = 40). The temperature profile was set at 230, 230, 220, 220, 200, 200, 200, and 200 °C from the hopper to the die (3 mm) [26]. The strands coming out of the extruder were then cooled in a water bath and pelletized (Thermo Fisher, Stone, UK). All the specimens for testing were molded using an Engel e-Victory injection molding machine with a 40-ton platen force [27, 28]. The temperature was fixed at 220 °C in the barrel and at 180 °C at the nozzle, while the mold was maintained at 45 °C [29, 30].

3 Characterization techniques

3.1 Scanning electron microscopy

In order to evaluate the morphology of the polymer blends a scanning electron microscopy (SEM) was recorded using EDAX Quanta 200, manufactured by FEI Company. SEM was used at different magnifications on samples previously cryofractured (liquid nitrogen). Before observation, the fractured surface was sputter coated with a thin gold coating to increase the surface conductivity.

Table 1 Materials used in this study

Material	Grade	Supplier	Comment
PA6	Ultramid O	BASF	Density = 1.13 g/cm^3 and melting temperature = 220 °C
ABS	Terpolymer	SODEVIC	Density = 1.04 g/cm^3 and melting temperature = 220 °C
SEBS-g-MA	Kraton F-G-1901-X	Shell	1.4 to 2 wt% maleic anhydrides

3.2 FTIR analysis

Fourier transform-infrared spectra of the blends were recorded using an ABB Bomem FTLA 2000-102 spectrometer (ATR: SPECAC GOLDEN GATE). The spectra were obtained by a superposition of 16 scans with a resolution of 4 cm^{-1}.

3.3 Thermal analysis

Differential scanning calorimetry (DSC) analysis was carried out using a Q100 instrument from TA Instruments. Test samples, weighing about 12 mg, were placed in an aluminum pan and heated, cooled, and heated again from − 50 to 230 °C at 10 °C/min. The first cycle was only used to delete the sample thermal history and was not analyzed.

3.4 Tensile testing

According to ISO 527-3 [19], tensile testing of five specimens from each type of blend polymer was performed. The tests were performed on a universal testing machine INSTRON 8821S (Instron, USA) at a crosshead speed of 5 mm/min using a 5-kN load cell. For mechanical characterization five tests (samples) were taken for each blend material, and the averages were used as representative values.

3.5 Dynamic mechanical thermal analysis

The RSA machine form TA Instruments was used to determine the dynamic mechanical thermal properties (DMTA) of the blends according to ASTM D 4092-01 [20]. Samples of 45 mm in length, 5.5 mm in width, and 2 mm in thickness were used in the dual cantilever configuration. The strain sweep test was performed at a frequency of 1 Hz. The frequency sweep test was ranged from 0.015 to 15 Hz at a set strain rate of 0.002 when the temperature sweep test was ranged from 30 to 120 °C with a heating rate, frequency, and strain at 5 °C/min, 1 Hz, and 0.002, respectively.

Table 2 ABS/PA6 Master bach formulation

		ABS (wt%)	PA6 (wt%)	Master bach (wt%)*
ABS/PA6-0 wt% SEBS-g-MA	0/100/0	0	100	0
	5/95/0	5	95	0
	15/85/0	15	85	0
	25/75/0	25	75	0
	35/65/0	35	65	0
	40/60/0	40	60	0
	45/55/0	45	55	0
	50/50/0	50	50	0
	55/45/0	55	45	0
	60/40/0	60	40	0
	65/35/0	65	35	0
	75/25/0	75	25	0
	85/15/0	85	15	0
	95/5/0	95	5	0
	100/0/0	100	0	0
ABS/PA6-8 wt% SEBS-g-MA	0/100/8	0	100	8
	5/95/8	5	95	8
	15/85/8	15	85	8
	25/75/8	25	75	8
	35/65/8	35	65	8
	40/60/8	40	60	8
	45/55/8	45	55	8
	50/50/8	50	50	8
	55/45/8	55	45	8
	60/40/8	60	40	8
	65/35/8	65	35	8
	75/25/8	75	25	8
	85/15/8	85	15	8
	95/5/8	95	5	8
	100/0/8	100	0	8
ABS/PA6-8 wt% SEBS-g-MA	0/100/16	0	100	16
	5/95/16	5	95	16
	15/85/16	15	85	16
	25/75/16	25	75	16
	35/65/16	35	65	16
	40/60/16	40	60	16
	45/55/16	45	55	16
	50/50/16	50	50	16
	55/45/16	55	45	16
	60/40/16	60	40	16
	65/35/16	65	35	16
	75/25/16	75	25	16
	85/15/16	85	15	16
	95/5/16	95	5	16
	100/0/16	100	0	16

*The value of SEBS-g-MA is taken for equivalent of 100 g blend (ABS/PA6)

3.6 Dynamic rheological measurements

Oscillatory melt rheology tests were performed on an MCR 500 (Physica) rheometer equipped with a CTD600 device. The measurements were carried out at 220 °C under small amplitude oscillatory shear mode using a 25-mm parallel plate-plate geometry with 2-mm-thick samples. Frequency sweeps between 500 and 0.5 Hz were performed at a strain of 5%, for which the materials exhibit a linear viscoelastic behavior as verified by previous strain sweeps.

4 Results and discussion

4.1 Blend morphology

In the relevant studies, SEM was successfully used to elucidate the compatibility of blends by observing the morphology, and degree of dispersion [31, 32]. Figure 1 presents typical morphologies of the blends with and without the compatibilizer. As expected, the morphology (texture) of the blend's changes with ABS content. At low dispersed phase content (15% ABS or 15% PA6), the morphology is mostly sea-island with a large amount of droplet phenomenon and droplet size close to 8 μm, which confirms that both polymers are immiscible. On the other hand, Fig. 1 (b, b′, c, c′) shows that the addition of SEBS-g-MA at 8 wt% may decrease the size of droplets to the average diameter of 5 μm leading to a formation of finer morphology with the presence of lower amount of pullout phenomenon as compared of neat ABS/PA6 material that may be ascribed to compatibilizing effect of SEBS-g-MA via the physical interaction engendering by the hydroxyl group. However, at high SEBS-G-MA loading (16 wt%), the morphology of blend starts to transform in a co-continuous structure with the presence of highly dispersed a small droplet with a size of 3 μm .This structure is due to the coalescence suppression of phase-separated domains through the formation of physical interaction between the polymer components via SEBS-g-MA [25]. In this case, any properties change as described next can be associated with better interfacial stress transfer due to better compatibility instead of changes related to the microstructure of the blends (morphologies).

4.2 Fourier transform infra-red spectroscopy analysis

FTIR spectra of PA6, ABS, and PA6 mixed with 50% by weight of ABS are shown in Fig. 2a. The spectrum of PA6/ABS blend shows the characteristic absorption of PA6 and ABS. The PA6 peak positions showing major absorption bands are 3307, 3088, 2925, and 2847 cm^{-1}. The broad absorption at 3307 and 3088 cm^{-1} corresponds to N–H hydrogen bond stretching vibration and N–H stretching, respectively [33]. The peak at 2925 cm^{-1} corresponds to CH_2 non-symmetric stretching vibration, and the peak at 2847 cm^{-1} is assigned to CH_2 symmetric stretching vibration [33] . The peak at 1637 cm^{-1} is assigned to carbonyl stretching vibration of amide I band. The peak at 1542 cm^{-1} corresponds to N–H bending and C–N stretching of amide II band [34]. On other hand, FTIR spectrum of ABS shows the hydroxyl groups (2635 cm^{-1}), carbonyl groups (1644 cm^{-1}), a broad region of C–O stretching vibrations (1000–1300 cm^{-1}) [35], the unsaturated groups from the polybutadiene phase of ABS corresponding to the peak of trans-1,4 (960 cm^{-1}), and vinyl-1,2 (908 cm^{-1}) [35]. The absorption band peak at 702 cm^{-1} corresponds to the out-of-phase bending vibration of the C–H bond of the aromatic ring [36]. It was observed from the spectrum of PA6/ABS blends that the characteristic bands of PA6 were not modified by the presence of ABS and no new band appeared which can explain that the chemical groups were not affected between PA6 and ABS.

Figure 2 b presents the FTIR spectra of PA6, SEBS-g-MA, and PA6/SEBS-g-MA blend. The spectra of tri-bloc SEBS grafted with maleic anhydride (SEBS-g-MA) showed the characteristic absorption bands at 2934, 2860, 1712, 1460, and 1020 cm^{-1} corresponding to C–H stretching asymmetric, symmetric, C=O stretching vibration, and symmetrical stretching vibration of the C–O–C ester groups in the maleic anhydride ring, respectively [37] . Also, the SEBS-g-MA spectrum shows two characteristics band at 1712 cm^{-1}, which is attributed to the symmetric and asymmetric vibration of saturated anhydride ring [38]. It can be seen in the FTIR spectrum of the (PA6/SEBS-g-MA) mixture at a weight ratio of 84/16 that the stretching vibration of C–O–C decreases strongly when SEBS-g-MA is added to the PA6 and the presence of the amide group was confirmed by the C–N and C–C stretching vibration in the region (1345–1235 cm^{-1}). The presence of amide bands and the decrease in starching band of MA indicate that the amide grafting reaction between PA6 and SEBS-g-MA occurred. During melt blending, anhydride acid functional groups of SEBS-g-MA react with the amine end groups of PA6 and also amide linkage, leading to SEBS-g-PA6 copolymer at the interface, enhancing interfacial adhesion between PA6 and SEBS-g-MA.

Figure 2 c shows the infrared spectrum of (PA6/SEBS-g-MA), ABS, and (PA6/SEBS-g-MA and ABS blend) at a weight ratio of 50/50. In the spectrum of PA6/SEBS-g-MA and ABS blend, it is seen that bands of this blend are the result of the superposition of the spectra of PA6/SEBS-g-MA and ABS. Indeed, the characteristic peaks of PA6/SEBS-g-MA and ABS appear with slight variations in area and intensity, which results in changes in interfacial interaction between PA6/SEBS-g-MA and ABS, and no chemical reaction is expected in this blend.

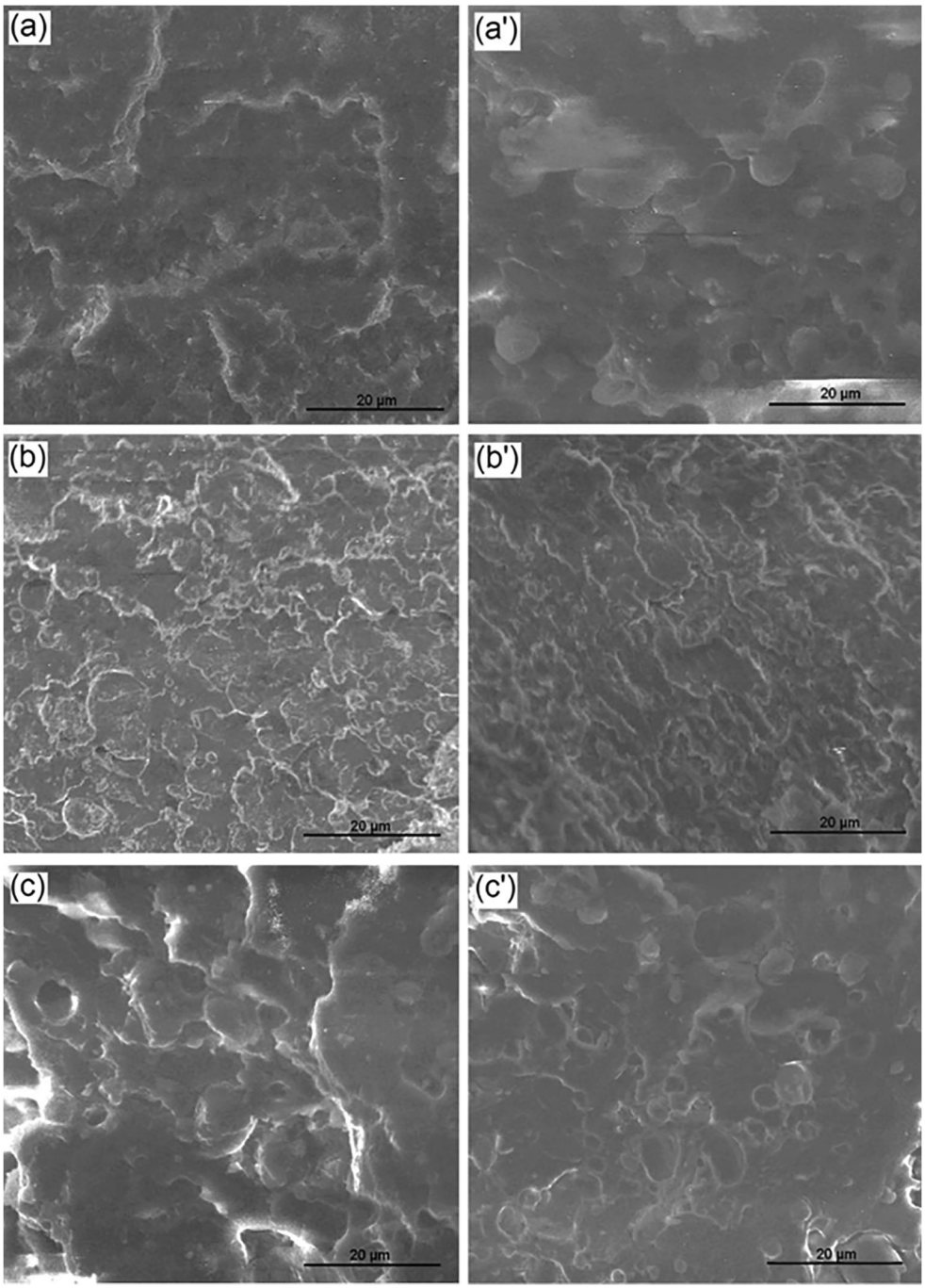

Fig. 1 Typical SEM images of selected blends: (a) 85PA6/15ABS, (a′) 85PA6-SEBS-g-MA/15ABS, (b) 50PA6/50ABS, (b′) 50PA6-SEBS-g-MA/50ABS, (c) 15PA6/85ABS, and (c′) 15PA6-SEBS-g-MA/85ABS

4.3 Differential scanning calorimetry

DSC was used to investigate the influence of the blend effect and the use of SEBS-g-MA on the melting temperature (T_m), specific enthalpy of melting (H_m), and crystallization temperature (T_c) (Table 4). In general, the crystallinity of the composite is related to the dispersed phase, which can act as nucleating agents in a polymer matrix. The polymer molecular chains can crystallize by themselves through a self-nucleation effect (homogeneous nucleation) or by introducing a nucleating agent (heterogeneous nucleation) [26, 39]. Semi-crystalline polyamide 6 may have its melting and crystallization behavior changed by the presence of a second component in polymer blends. Any significant modification of PA6 melting and/or crystallization behavior in the blend can lead to properties changes of the resulting material. PA6 molecular grafting, due to reactive compatibilization, may modify its kinetics of crystallization, which would lead to different crystal dimensions and different degree of crystallinity compared with neat PA6. Parameters such as melting temperature (T_m),

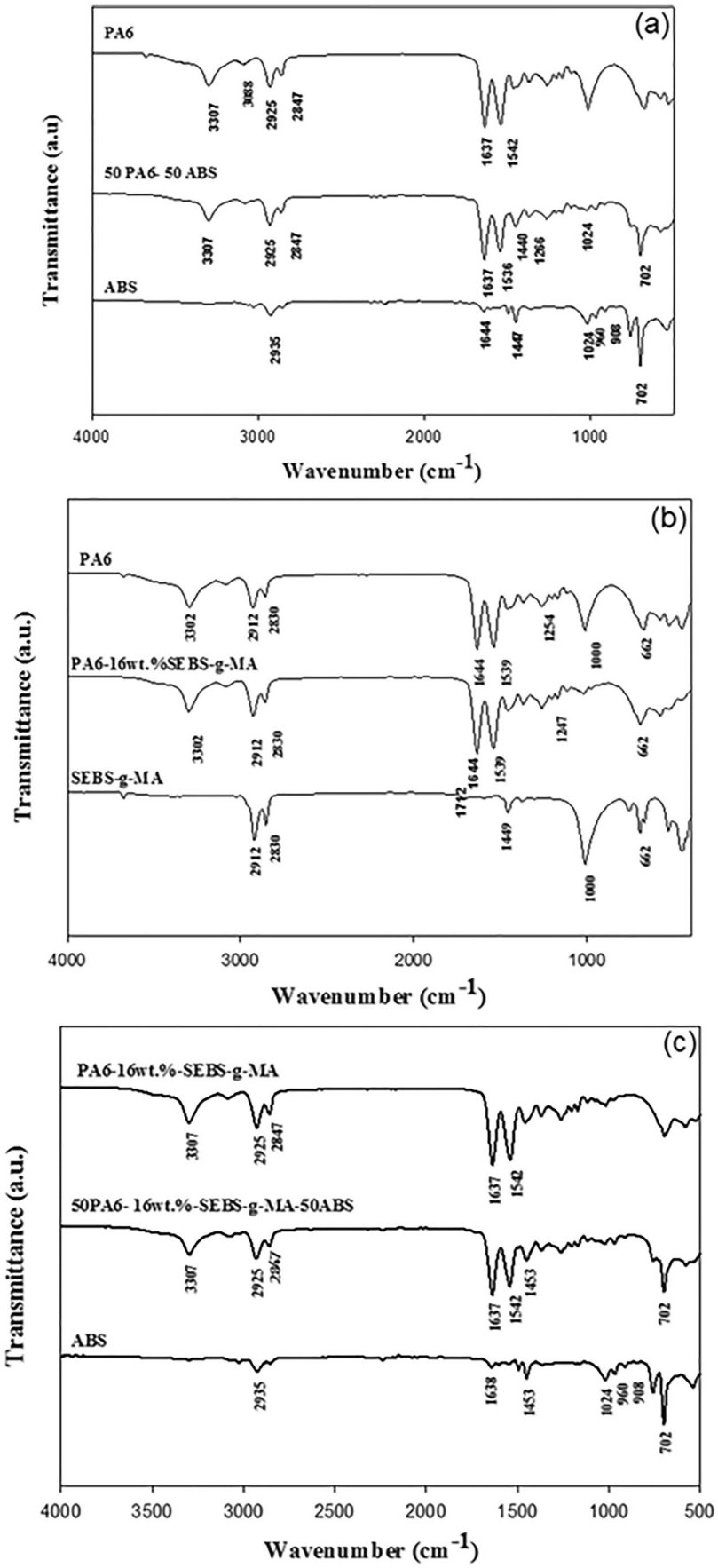

Fig. 2 FTIR spectrum of **a** PA6, ABS, and 50PA6/50 ABS blend; **b** PA6, SEBS-g-MA, and PA6-16 wt% SEBS-g-MA; and **c** PA6-16 wt% SEBS-g-MA, ABS, and 50PA6-16 wt%-SEBS-g-MA/50 ABS

crystallization temperature (T_c), and heat of fusion (H_m) were used to observe changes in melting and crystallization behavior of PA6 compatibilized by SEBS-g-MA blends with ABS. Table 3 presents these results.

The addition of ABS to PA6 did not change the melting temperature (T_m). However, the heat of fusion (H_m) was affected only for higher amounts of ABS in the binary blends. During cooling, the crystallization temperature (T_c) decreased when ABS is blended with PA6. Therefore, there is evidence that ABS with a lower crystallinity interferes in the crystallization of PA6.

The results show that the heat of fusion (H_m) for the ternary blends is lower than that for binary ones. However, changes in T_m values for the ternary blends are not significant. That trend is similar for both change in the blend composition and the amount of SEBS-g-MA copolymer. Therefore, decrease of heat of fusion could be a result of partial miscibility between ABS and grafted PA6-g-SEBS-MA molecules. There was also a depression in the crystallization temperature with the use of the compatibilizer. The rubber (amorphous) character of SEBS-g-MA copolymers can strongly affect PA6 melting and crystallization in PA6/SEBS-g-MA/ABS ternary blends.

4.4 Tensile properties

4.4.1 Young's modulus

The addition of ABS into PA6 leads to a significant change of its mechanical properties. Increasing ABS content from 0 to 100 wt% resulted in increasing Young's modulus from 931 MPa for neat PA6 to 1800 MPa for neat ABS (Fig. 3a). This is due to the higher rigidity of ABS compared with PA6 and ABS, which is acting as a reinforcement agent. It is also observed in Fig. 3b, c that the use of a compatibilizer increases the Young's modulus of the blends. This can be ascribed to better stress transfer at the interface since SEBS-g-MA has a very low elastic modulus around 7.2 MPa [40, 41]. The experimental values of Young's modulus were compared with two commonly used theoretical models, which are Voigt and Reuss [42] :

$$\begin{cases} E_{//} = V_A E_A + (1-V_A)E_B \\ E_{\perp} = \dfrac{E_A E_B}{V_A E_B + (1-V_A)E_A} \end{cases}$$

where $E_{//}$ is Voigt model and $E_{\perp}$ is Reuss model, and E_A; E_B are the elastic modulus of the phases A and B, respectively, and are the volume fraction.

These models are generally used to approximate the mechanical behavior of blend materials/blends. The Voigt model can be viewed as an upper limit, while Reuss model should represent the lower limit. Most of the time, the degree of compatibility and adhesion between the continuous and dispersed phases control the final results between these limits. It can be clearly observed in Fig. 3a that the Young's modulus for the uncompatibilized blends is in agreement with Reuss model. On the other hand, the data are more closely in agreement with Voigt model with increasing compatibilizer content. It can be deduced that the addition of SEBS-g-MA enhanced the adhesion between ABS and PA6 so to improve compatibility and modulus.

Since the highest coupling agent content (16 wt%) gives results close to the Voigt model over all the ABS concentration range, this value can be considered as the optimum.

Table 3 DSC results of PA6/ABS blends with and without SEBS-g-MA

Sample ABS/PA6-wt% SEBS-g-MA	Hm (J/g)	Tm (°C)	Tc (°C)
100/0/0	22.3	225	180
0/100/0	75.5	221	190
15/85	72.1	222.1	188.6
15/85/8	60.8	221.2	188.3
50/50	51.8	222.3	188.2
50/50/8	42.0	221.8	187.5
85/15	33.9	222.5	186.6
85/15/8	23.9	221.1	184.7

4.4.2 Tensile strength

The tensile strength represents the maximum amount of tensile stress that a material can sustain before failure starts. For all blend system the curves are normalized and show that for all the blends (PA6/ABS with and without SEBS-g-MA), the tensile strength generally increases with ABS and SEBS-g-MA contents (Fig. 4; Table 4). The slight decreases at low ABS content can be related to possible stress concentration generated by the sea-island morphology created and decohesion of the phases, especially at low compatibilizing agent content (0 and 8%). The position and the value of this minimum depend on coupling agent content. On the other hand, the following increase in the curves can be explained by the creation of a co-continuous morphology in the blends. At higher SEBS-g-MA content (16%), the minimum disappears indicating again a better stress transfer at the interface which seems to be optimally compatibilized which confirms again the previous trends observed since the use of reactive compatibilizers in immiscible blends often leads to higher interfacial area and higher entanglement at the interface leading to improved tensile properties [43]. The amine group at the end of PA6 macromolecule is capable of reacting with maleic anhydride groups in SEBS-g-MA and forms grafted copolymer at interface of the blends. These interactions can stabilize the interface by reducing the interfacial tension,

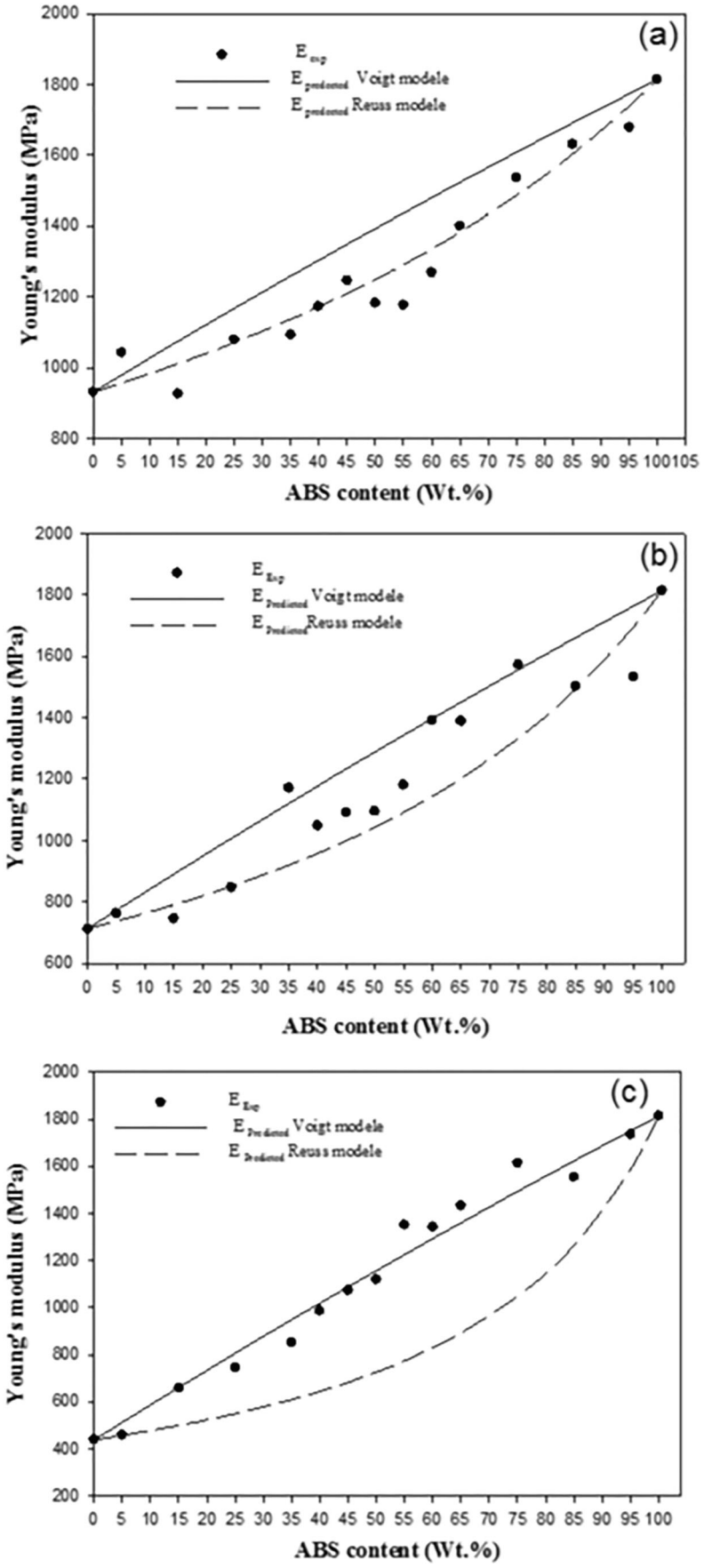

Fig. 3 Experimental and predicted Young's modulus of PA6/ABS blends as a function of ABS content with **a** 0, **b** 8, and **c** 16 wt% SEBS-g-MA

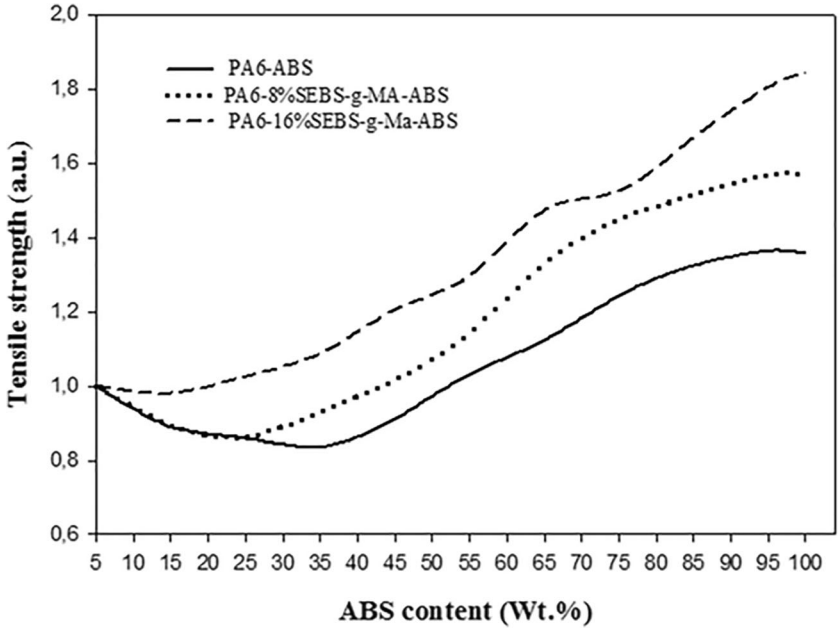

Fig. 4 Tensile strength of the blends as a function of ABS and SEBS-g-MA contents

resulting in enhancement of the interfacial viscosity and adhesion. This is the reason why those compatibilized ABS/PA6 blends exhibited higher tensile strength than uncompatibilized ABS/ PA6 blends.

4.5 Dynamic mechanical thermal analysis

4.5.1 Frequency sweep

DMTA analysis has been used in the past to determine the boundary of co-continuity because the mechanical properties are susceptible to the morphology of blends since the continuous phase is mainly controlling the stiffness of the sample [44, 45].

Dynamic frequency sweeps were performed at a 0.002 strain amplitude to stay in the linear viscoelastic range of the materials, and Fig. 5 presents the values of complex modulus and mechanical loss factor (tan δ) at different frequencies (0.015, 0.15, 1.5, and 15 Hz) as a function of ABS and SEBS-g-MA contents. It can be seen that the trends are similar for all the curves[45].

According to Fig. 5, it is clear that the complex modulus increases with ABS content and frequencies, indicating that

Table 4 Tensile strength of different composite formulation

Composites formulation (ABS/PA6)	Tensile strength (MPa/ MPa) ABS/PA6-0 wt% SEBS-g-MA	Tensile strength ABS/PA6-8 wt% SEBS-g-MA	Tensile strength ABS/PA6-16 wt% SEBS-g-MA
5/95	1	1	1
15/85	0.8896	0.8947	0.9800
25/75	0.8580	0.8620	1.0262
35/65	0.8353	0.9295	1.0874
40/60	0.8683	0.9352	1.1435
45/65	0.9116	1.0163	1.2066
50/50	0.9774	1.0774	1.3231
55/45	1.0316	1.1437	1.2965
60/40	1.0734	1.2162	1.3867
65/35	1.1246	1.3303	1.4753
75/25	1.2431	1.4487	1.5147
85/15	1.3248	1.5153	1.6699
958	1.3637	1.5690	1.8058
100/0	1.3561	1.5688	1.8445

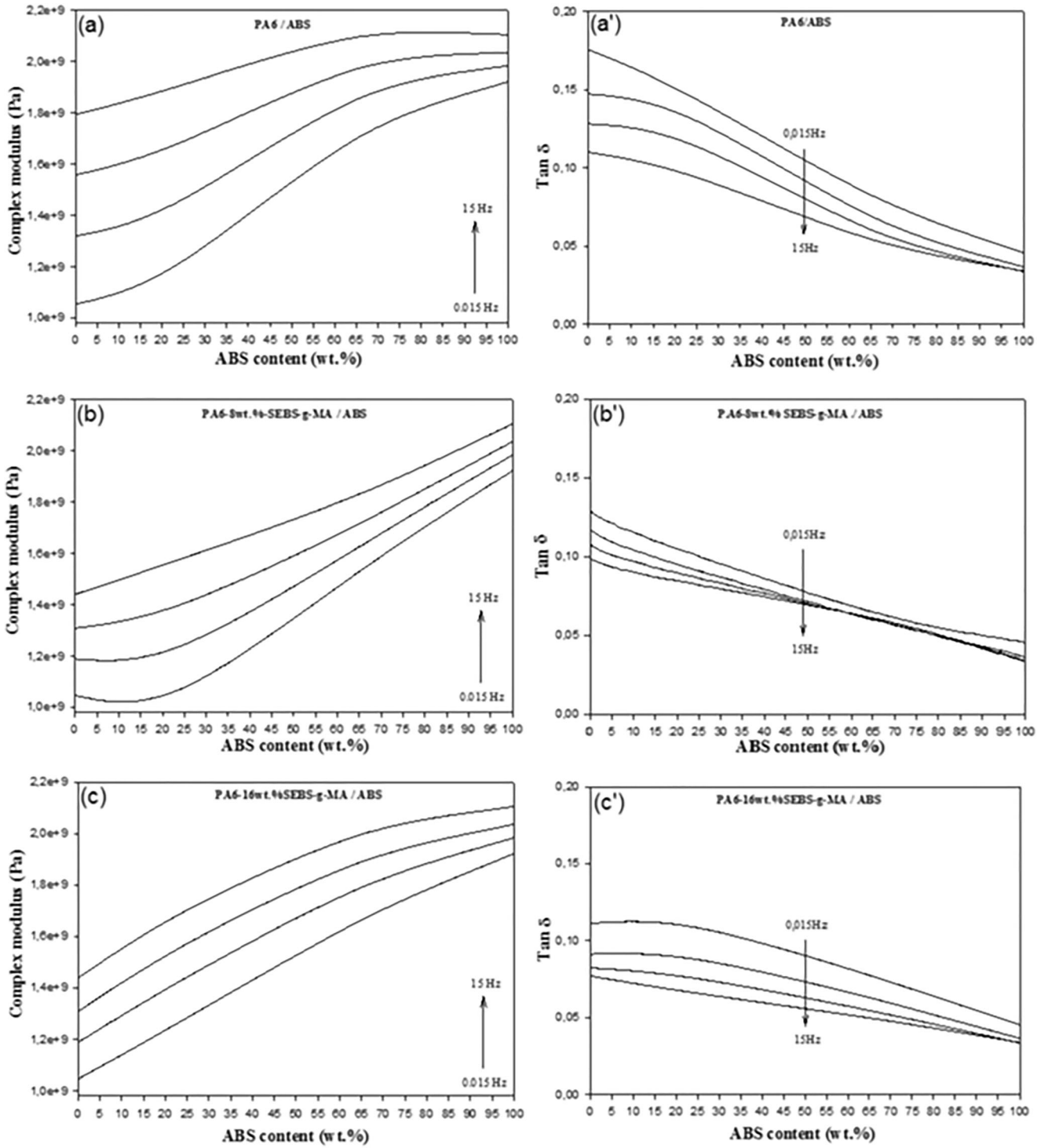

Fig. 5 Complex modulus as a function of ABS content: (a) 0, (b) 8, and (c) 16 wt% SEBS-g-MA; as well as the value of the damping factor (tan δ as a function of ABS content: (a′) 0, (b′) 8, and (c′) 16 wt%. Different curves represent different frequencies

the relaxation time decreases with the addition of ABS and increasing frequency [29, 46]. It can be observed that ABS content has a significant influence on the complex modulus of the blends. Thus, ABS cause a remarkable increase in the complex modulus, which is attributed to the increase in the polymer chain displacement and the change in the molecular dynamics. This is presumably due to a reinforcing effect of the interface by the presence of ABS, which play the reinforcement role. Figure 5 shows that for the systems studied, the complex modulus (E^*) increases, while the loss factor (tan

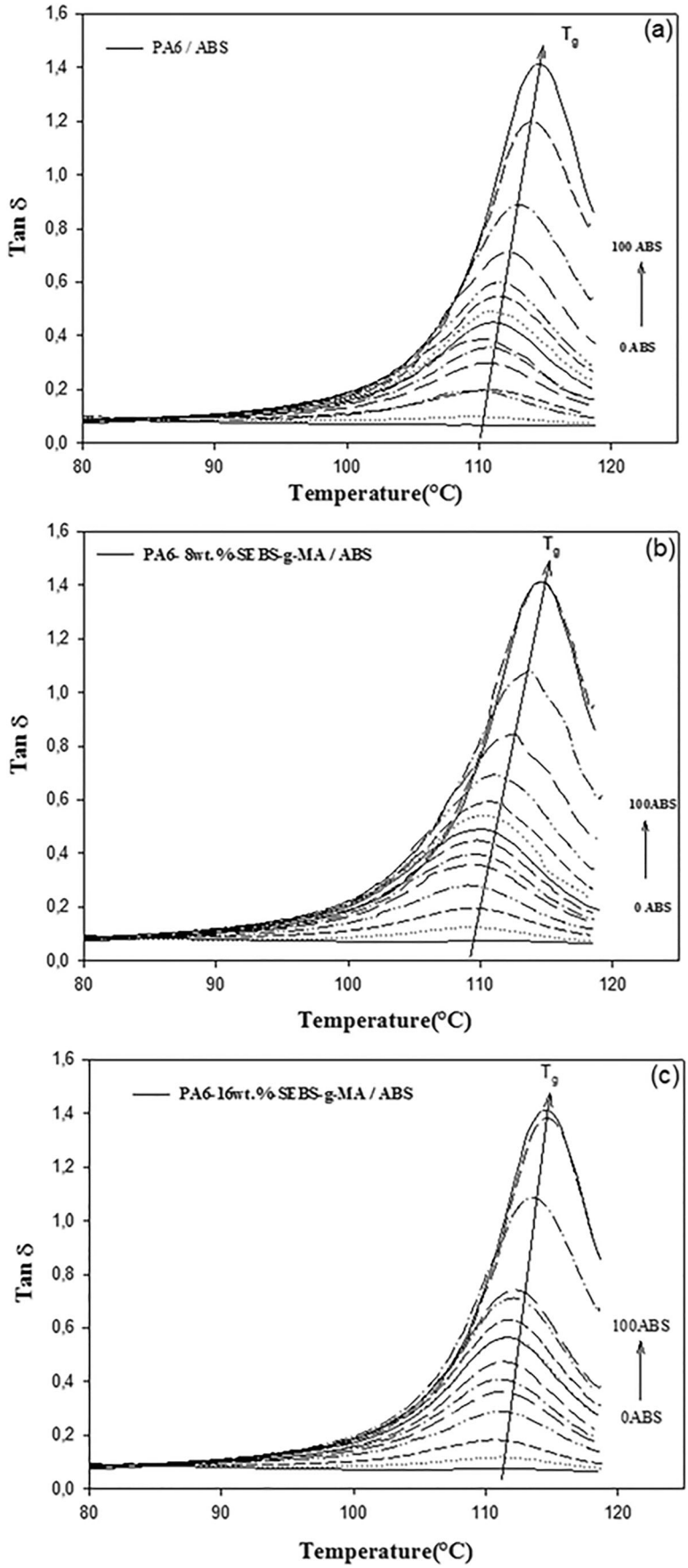

Fig. 6 Damping factor (tan δ) as a function of temperature for different ABS content with **a** 0, **b** 8, and **c** 16 wt% SEBS-g-MA

Table 5 Glass transition temperature as a function of ABS and SEBS-g-MA contents

ABS content (wt%)	Glass transition temperature (°C)		
	0 wt% SEBS-g-MA	8 wt% SEBS-g-MA	10 wt% SEBS-g-MA
0	40.2	47.0	47.0
5	49.0	109.7	48.2
15	110.8	109.4	110.7
25	110.8	109.0	111.0
35	110.8	109.3	111.1
40	110.8	109.4	110.8
45	110.8	109.6	111.1
50	111.1	109.9	111.5
55	111.1	110.2	111.5
60	111.3	110.5	111.8
65	111.7	111.1	112.1
75	112.2	112.6	112.1
85	113.0	113.6	113.6
95	114.0	114.4	114.6
100	114.7	114.7	114.7

δ) decreases with frequency [29, 46]. This is attributed to the fact that the molecular chains, for this range of frequency, have not enough time to respond to the applied strain, so the rigidity increases with increasing frequency, i.e., the elastic character of the material prevails over its viscous behavior.

It was also observed that the complex modulus is much more sensitive to ABS content than the loss factor. A change in the tan δ curve indicates a relaxation process, and it is associated with the motion of small groups and chains of molecules within the polymer structure.

4.5.2 Temperature sweep

Damping factor (tan δ) is closely connected to the impact strength of the material. The material changes from a solid state to a viscous state depending on the movement of its constituent groups and the main polymer chain structures. The variation of tan δ of the uncompatibilized and compatibilized systems as a function of temperature is shown in Fig. 6. Tan δ was almost constant at low temperature but increases substantially with temperature, which corresponds to higher damping due to the initiation of motion in segments of the main polymer chain[30] . The temperature at which the tan δ peak occurs is commonly reported as the glass transition temperature (T_g). Otherwise, if the interfacial adhesion is poor, applied energy will be dissipated in the form of heat due to the interaction between the polymers. Consequently, the peak of tan δ (T_g) is increased with decreasing the interfacial adhesion. The results reported in Table 2 show that increasing ABS content shift the tan δ curve peaks to higher temperature for all the systems studied. T_g increase rapidly between 0 and 15 wt% ABS; i.e., from 40 °C (T_g of neat PA6) to reach 110 °C (Table 5). Then, a plateau in the range 15–100 wt% ABS is observed. In the blend systems, the increasing of T_g is due to incorporation of ABS, resulting in an improvement in damping and showing that the blend polymer composites are more elastic; the elastic behavior became more prominent with the highest amount of ABS due to the higher intrinsic rigid character of Abs against PA6 and SEBS-g-MA.

In the other hand, it is clear that the T_g increase became more rapid when coupling agent was added. Indeed, T_g increased from 47 (T_g of compatibilized PA6) to 109 °C as the ABS content has increased only from 0 to 5 wt%. This increase in T_g is probably related to a change to a co-continuous morphology with the addition of the compatibilizer [45, 47]; i.e., a blend with poor interfacial bonding tends to dissipate more energy than good interfacial bonding; if the interfacial adhesion is poor, applied energy will be dissipated in the form of heat due to the interaction between the polymers [45, 47] . The increase in T_g is taken as a measure of interfacial interaction. Furthermore, these effects are enhanced at higher SEBS-g-MA content, when using a coupling agent, the polymer matrix become more ductile, and the effective energy dissipation mechanism in the brittle binary blend increases. As a contrast, the brittle-ductile transition occurs with the incorporation of SEBS-g-MA. These results confirm again that better compatibility or miscibility is obtained in the blends with the addition of coupling agent.

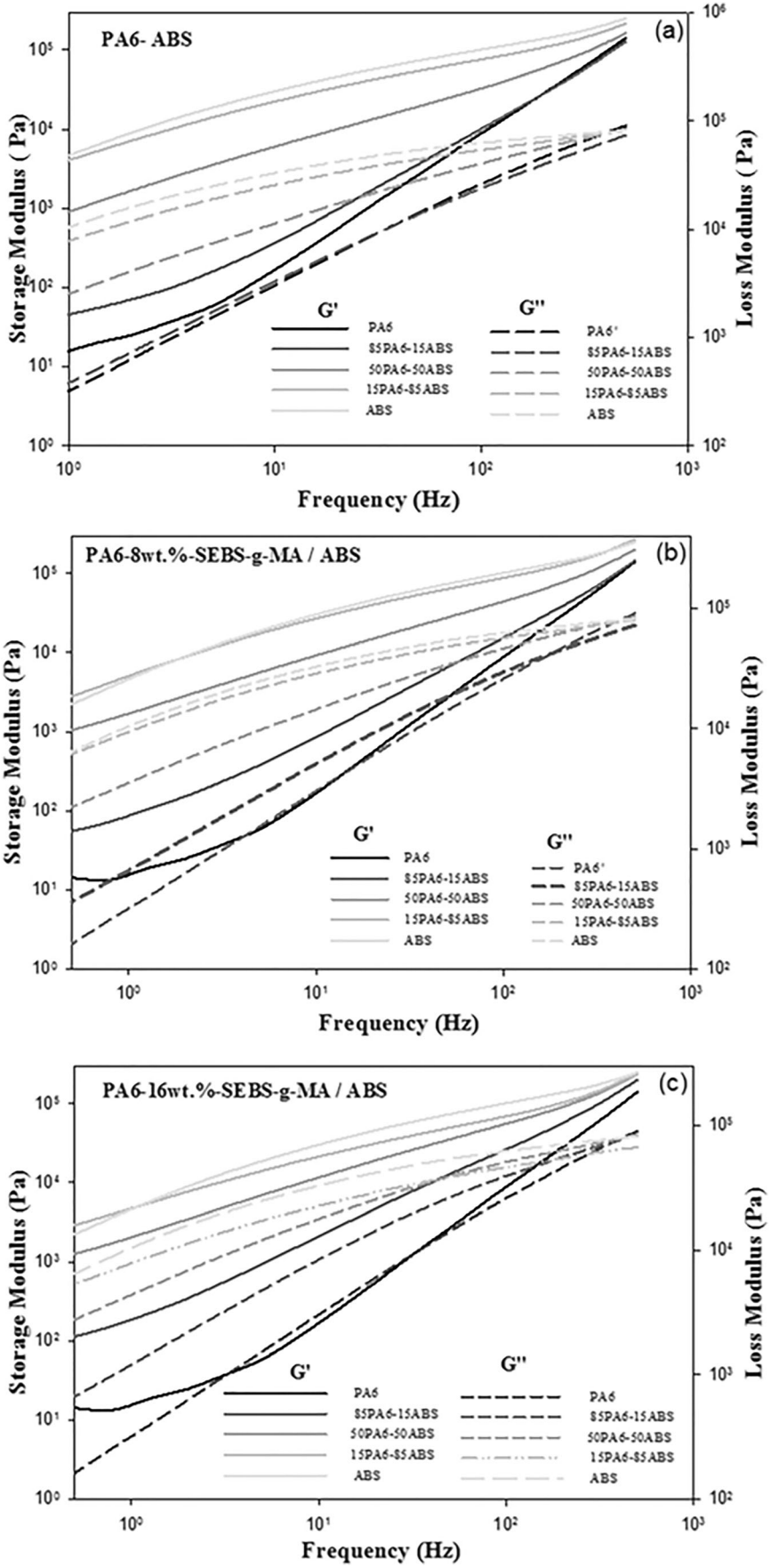

Fig. 7 Storage and loss moduli as a function of frequency for different ABS content with **a** 0, **b** 8, and **c** 16 wt% SEBS-g-MA

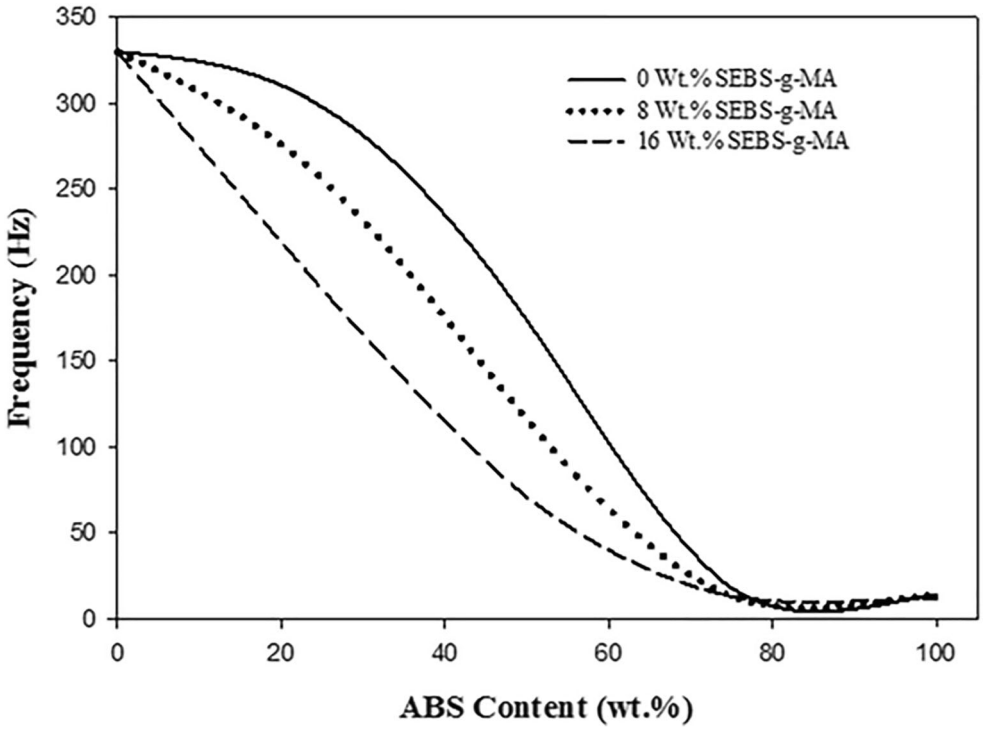

Fig. 8 Crossover frequency ($G' = G''$) as a function of ABS and SEBS-g-MA contents

4.6 Rheological properties

4.6.1 Storage modulus and loss modulus

The curves of dynamic storage modulus (G') and loss modulus (G'') as a function of angular frequency (ω) are presented in Fig. 7 for the different blends with and without compatibilizer. It is evident that both G' and G'' increase with increasing angular frequency, which is in agreement with DMTA results. The addition of ABS increases G' and G'' revealing the reinforcing effect of ABS. It is also observed for all the blends that at high frequency, G' values are higher than G'' indicating a more solid-like response in molten state, while the reverse occurs at low frequency. This behavior is due to insufficient time at higher frequency to allow polymer chains to relax which contributed to an increase in the elastic nature of the polymer melt. Hence, the solid-like behavior indicates strong interactions between the components [48].

According to the crossover point were $G' = G''$ (Fig. 8), this condition indicates a transition from an elastic to a viscous behavior; i.e., the blend composites at the crossover points have the same viscous and elastic behavior. It was observed that increasing the rigid content, ABS phase in the polymer matrix (PA6) decreases the crossover frequency. The results indicate a decreasing crossover frequency from 330(neat PA6) to 12 Hz (neat ABS) indicating the reinforcing effect of ABS leading to a higher elastic behavior of melt. Lower crossover frequency indicates an increase of the relaxation time of the polymer [26, 49]. Beyond the crossover point, G'' becomes smaller than G' and shows a plateau-like non terminal behavior, which implies an elastic behavior of the melt. The addition of ABS disturbs the mobility of polymer chains in the melt, thus increasing the storage modulus and loss modulus of the blend confirming the reinforcement effect of ABS. On the other hand, it can be clearly seen that the rheological properties of the blend show a predominantly viscous behavior at low frequencies ($G' < G''$), and a more elastic behavior at high frequencies ($G' > G''$) which is due to the polymer chains relaxation time.

Also, a closer examination and comparison of the blend composites response with and without coupling agent reveals a very interesting effect of the coupling agent microstructure on the polymer chain response [26, 49]. A shift of the crossover frequency is observed with compatibilizer addition. Higher frequency at higher SEBS-g-MA contents indicates a lower relaxation time of the blend. SEBS-g-MA is a coupling agent characterized by a rubber support (SEBS) with a ductile behavior and the MA, which ensure the adhesion [41]. This coupling agent effect is further supported by the rheological curves where the blend composites with coupling agent show a more viscous behavior. The observed shift in crossover frequency can be associated with the combined effect of the compatibilizer with it rubber character and changes at the blend matrix interface and makes the processing and blending of composites, easier.

4.6.2 Complex viscosity

The melt rheological response for the blends with and without compatibilizer is presented in Fig. 9 Neat PA6 shows mainly a

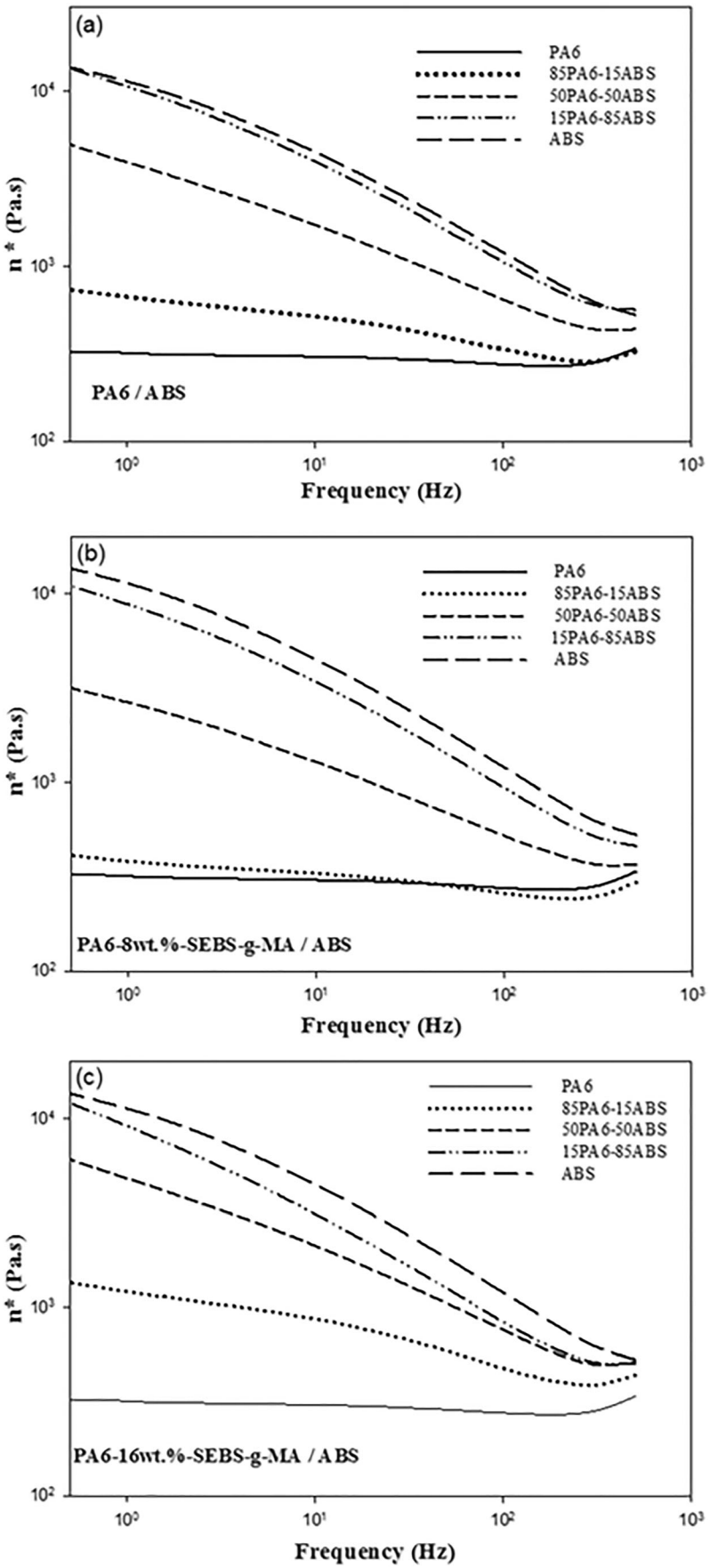

Fig. 9 Complex viscosity as a function of frequency for different ABS content with **a** 0, **b** 8, and **c** 16 wt% SEBS-g-MA

Newtonian flow behavior in the measured frequency range as complex viscosity is found to be independent of the frequency. In addition, the melt viscosity of the blends increases with increasing ABS content. Globally, the increase of ABS content percentage in the (PA6-ABS) blend, with or without compatibilizer, leads to an increase in viscosity. This has been due certainly to the higher viscosity of neat ABS. With the addition of the coupling agent, a slight increase in melt viscosity is observed for the compatibilized blends. The observed increase in melt viscosity can be associated to the effect of the compatibilizer, changing the rheological behavior of the interphase [26, 50]. Here again, the melt state data (Figs. 8 and 9) confirm the results obtained in the solid state (Figs. 2, 3, 4, 5, 6, and 7); i.e., PA6 properties increase with ABS and SEBS-g-MA contents

5 Conclusion

The structural, morphological, mechanical, and rheological properties of PA6/ABS blends were studied considering the effect of ABS content and SEBS-g-MA content as 8 and 16 wt% contents. The amount of compatibilizer was found to have significant effect on the mechanical and rheological properties; it was exhibited that the tensile strength improved upon the addition of compatibilizer. Dynamic mechanical thermal analysis confirmed the system immiscibility and determined the T_g of the two phases in the polymer blend. It was observed a slight increase in the T_g with addition of ABS and compatibilizer. The processing property of the blends systems was investigated by using dynamic rheometer analysis. The rheological measurement shows the increased adhesion interfacial between the blend's components. In the other hand, addition of ABS in PA6 (uncompatibilized and compatibilized) increases the storage and loss modulus as well as the complex viscosity of the blend's material.

References

1. Okonkwo EG, Anabaraonye CN, Daniel-Mkpume CC, Egoigwe SV, Okeke PE, Whyte FG, Okoani AO (2020) Mechanical and thermomechanical properties of clay-Bambara nut shell polyester bio-composite. Int J Adv Manuf Technol 108:2483–2496. https://doi.org/10.1007/s00170-020-05570-w
2. Gbadeyan OJ, Mohan TP, Kanny K (2020) Processing and characterization of 3D-printed nanoclay/acrylonitrile butadiene styrene (abs) nanocomposite gear. Int J Adv Manuf Technol 109:619–627. https://doi.org/10.1007/s00170-020-05648-5
3. Fen Yong W, Zhang H (2020) Recent advances in polymer blend membranes for gas separation and pervaporation. Prog Mater Sci 100713:100713. https://doi.org/10.1016/j.pmatsci.2020.100713
4. Yousef BF, Mourad AHI, Hilal-Alnaqbi A (2013) Modeling of the mechanical behavior of polyethylene/polypropylene blends using artificial neural networks. Int J Adv Manuf Technol 64:601–611. https://doi.org/10.1007/s00170-012-4069-4
5. Agboola O, Sunday O, Fayomi I et al (2020) Materials today: Proceedings polymers blends for the improvement of nanofiltration membranes in wastewater treatment: a short review. Mater Today Proc. https://doi.org/10.1016/j.matpr.2020.05.387
6. Kuo CFJ, Wu YS (2006) Optimization of the film coating process for polymer blends by the grey-based Taguchi method. Int J Adv Manuf Technol 27:525–530. https://doi.org/10.1007/s00170-004-2217-1
7. Balderrama-Armendariz CO, MacDonald E, Roberson DA, Ruiz-Huerta L, Maldonado-Macias A, Valadez-Gutierrez E, Caballero-Ruiz A, Espalin D (2019) Folding behavior of thermoplastic hinges fabricated with polymer extrusion additive manufacturing. Int J Adv Manuf Technol 105:233–245. https://doi.org/10.1007/s00170-019-04196-x
8. Wei B, Lin Q, Zheng X, Gu X, Zhao L, Li J, Li Y (2019) Reactive splicing compatibilization of immiscible polymer blends: compatibilizer synthesis in the melt state and compatibilizer architecture effects. Polymer (Guildf) 185:121952. https://doi.org/10.1016/j.polymer.2019.121952
9. Daitx TS, Jacoby CG, Ferreira CI, Schneider PH, Mauler RS (2019) Kaolinite-based Janus nanoparticles as a compatibilizing agent in polymer blends. Appl Clay Sci 182:105291. https://doi.org/10.1016/j.clay.2019.105291
10. Zuo X, Xue Y, Zhou Y, Yin Y, Li TD, Wang L, Chuang YC, Chang CC, Rafailovich MH, Guo Y (2020) The use of low cost, abundant, homopolymers for engineering degradable polymer blends: compatibilization of poly(lactic acid)/styrenics using poly(methyl methacrylate). Polymer (Guildf) 186:122010. https://doi.org/10.1016/j.polymer.2019.122010
11. You W, Yu W (2019) Viscoelastic characterization of compatibilized polymer blends. In: Compatibilization of polymer blends: micro and nano scale phase morphologies, interphase characterization, and properties. Elsevier, pp 435–452
12. Mayer AC, Scully SR, Hardin BE, Rowell MW, McGehee MD (2007) Polymer-based solar cells. Mater. Today 10:28–33
13. Wang M, Wang H, Li W, Hu X, Sun K, Zang Z (2019) Defect passivation using ultrathin PTAA layers for efficient and stable perovskite solar cells with a high fill factor and eliminated hysteresis. J Mater Chem A 7:26421–26428. https://doi.org/10.1039/c9ta08314f
14. Hu X, Wang H, Wang M, Zang Z (2020) Interfacial defects passivation using fullerene-polymer mixing layer for planar-structure perovskite solar cells with negligible hysteresis. Sol Energy 206:816–825. https://doi.org/10.1016/j.solener.2020.06.057
15. Almeida F De, Correia A, Silva ECE, et al (2018) Compatibilization effect of organophilic clays in PA6/PP polymer blend. In: Procedia manufacturing. Elsevier B.V., pp 1154–1161
16. Zhao D, Yan D, Fu X, Zhang N, Yang G (2020) Effect of ABS types on the morphology and mechanical properties of PA6/ABS blends by in situ reactive extrusion. Mater Lett 274:128013. https://doi.org/10.1016/j.matlet.2020.128013
17. Zhao D, Yan D, Zhang N, Yang G (2019) Preparation of supertoughened PA6 with submicron-sized ABS by in situ reactive extrusion method. Mater Lett 251:18–22. https://doi.org/10.1016/j.matlet.2019.05.029
18. Zhang Z, Cao M, Chen P, Yang B, Wu B, Miao J, Xia R, Qian J (2019) Improvement of the thermal/electrical conductivity of PA6/PVDF blends via selective MWCNTs-NH2 distribution at the interface. Mater Des 177:107835. https://doi.org/10.1016/j.matdes.2019.107835
19. Liu XQ, Bao RY, Liu ZY, Yang W, Xie BH, Yang MB (2013) Effect of nano-silica on the phase inversion behavior of immiscible PA6/ABS blends. Polym Test 32:141–149. https://doi.org/10.1016/j.polymertesting.2012.09.003
20. Arsad A, Rahmat AR, Hassan A, Iskandar SN (2011) Mechanical and rheological characterization of PA6 and ABS blends-with and

without short glass fiber. J Appl Sci 11:2313–2319. https://doi.org/10.3923/jas.2011.2313.2319
21. Sharma V, Kapoor S, Goyal M, Jindal P (2020) Enhancement of the mechanical properties of graphene based acrylonitrile butadiene styrene (ABS) nanocomposites. Mater Today Proc 28:1744–1747. https://doi.org/10.1016/j.matpr.2020.05.155
22. Zhou C, Yu W (2003) A rheological model for the interface of immiscible polymer melt in blending process. Can J Chem Eng 81:1067–1074. https://doi.org/10.1002/cjce.5450810519
23. Shen J, Piunova VA, Nutt S, Hogen-Esch TE (2013) Blends of polystyrene and poly(n-butyl methacrylate) mediated by perfluorocarbon end groups. Polymer (Guildf) 54:5790–5800. https://doi.org/10.1016/j.polymer.2013.08.059
24. Qaiss A, Bouhfid R, Essabir H (2015) Characterization and use of coir, almond, apricot, argan, shells, and wood as reinforcement in the polymeric matrix in order to valorize these products
25. Nekhlaoui S, Essabir H, Kunal D, Sonakshi M, Bensalah MO, Bouhfid R, Qaiss A (2015) Comparative study for the talc and two kinds of moroccan clay as reinforcements in polypropylene-SEBS- *g*-MA matrix. Polym Compos 36:675–684. https://doi.org/10.1002/pc.22986
26. Essabir H, Rodrigue D, Bouhfid R, Qaiss AEK (2016) Effect of nylon 6 (PA6) addition on the properties of glass fiber reinforced acrylonitrile-butadiene-styrene. Polym Compos. 39:14–21. https://doi.org/10.1002/pc.23895
27. Boujmal R, Essabir H, Nekhlaoui S, et al (2014) Composite from polypropylene and henna fiber: structural, mechanical and thermal properties. J Biobased Mater Bioenergy 8. https://doi.org/10.1166/jbmb.2014.1420
28. Essabir H, Raji M, Laaziz SA, Rodrique D, Bouhfid R, Qaiss A (2018) Thermo-mechanical performances of polypropylene biocomposites based on untreated, treated and compatibilized spent coffee grounds. Compos Part B Eng 149:1–11. https://doi.org/10.1016/j.compositesb.2018.05.020
29. Bensalah H, Gueraoui K, Essabir H, Rodrigue D, Bouhfid R, Qaiss A (2017) Mechanical, thermal, and rheological properties of polypropylene hybrid composites based clay and graphite. J Compos Mater 51:3563–3576. https://doi.org/10.1177/0021998317690597
30. Malha M, Nekhlaoui S, Essabir H, Benmoussa K, Bensalah MO, Arrakhiz FE, Bouhfid R, Qaiss A (2013) Mechanical and thermal properties of compatibilized polypropylene reinforced by woven doum. J Appl Polym Sci 130:4347–4356. https://doi.org/10.1002/app.39619
31. Essabir H, Hilali E, El Minor H et al (2015) Mechanical and thermal properties of polymer composite based on natural fibers: Moroccan Luffa sponge/high density polyethylene. J Biobased Mater Bioenergy 9:9–357. https://doi.org/10.1166/jbmb.2015.1524
32. Kakou CA, Essabir H, Bensalah M-O, Bouhfid R, Rodrigue D, Qaiss A (2015) Hybrid composites based on polyethylene and coir/oil palm fibers. J Reinf Plast Compos 34:1684–1697. https://doi.org/10.1177/0731684415596235
33. Pelin CE, Pelin G, Ştefan A et al (2016) Mechanical properties of polyamide/carbon-fiber-fabric composites. Mater Technol 50:723–728. https://doi.org/10.17222/mit.2015.171
34. Kusmono, Mohd Ishak ZA, Chow WS et al (2008) Influence of SEBS-g-MA on morphology, mechanical, and thermal properties of PA6/PP/organoclay nanocomposites. Eur Polym J 44:1023–1039. https://doi.org/10.1016/j.eurpolymj.2008.01.019
35. Bai X, Isaac DH, Smith K (2007) Reprocessing acrylonitrile–butadiene–styrene plastics: structure–property relationships. Polym Eng Sci 47:120–130. https://doi.org/10.1002/pen.20681
36. Bokria JG, Schlick S (2002) Spatial effects in the photodegradation of poly(acrylonitrile-butadiene-styrene): a study by ATR-FTIR. Polymer (Guildf) 43:3239–3246. https://doi.org/10.1016/S0032-3861(02)00152-0
37. Chen G, Shen D, Feng M, Yang M (2004) An attenuated total reflection FT-IR spectroscopic study of polyamide 6/clay nanocomposite fibers. Macromol Rapid Commun 25:1121–1124. https://doi.org/10.1002/marc.200400079
38. Infrared and Raman characteristic group frequencies: tables and charts, 3rd Edition. Wiley. https://www.wiley.com/en-us/Infrared+and+Raman+Characteristic+Group+Frequencies%3A+Tables+and+Charts%2C+3rd+Edition-p-9780470093078. Accessed 21 Jun 2020
39. Raji M, Essabir H, Rodrigue D, Bouhfid R, Qaiss A (2017) Influence of graphene oxide and graphene nanosheet on the properties of polyvinylidene fluoride nanocomposites. Polym Compos 39:2932–2941. https://doi.org/10.1002/pc.24292
40. Essabir H, Raji M, Essassi EM, Rodrigue D, Bouhfid R, Qaiss A (2017) Morphological, thermal, mechanical, electrical and magnetic properties of ABS/PA6/SBR blends with Fe3O4 nano-particles. J Mater Sci Mater Electron 28:17120–17130. https://doi.org/10.1007/s10854-017-7639-2
41. Essabir H, Bensalah MO, Rodrigue D, Bouhfid R, Qaiss A (2016) Biocomposites based on Argan nut shell and a polymer matrix: effect of filler content and coupling agent. Carbohydr Polym 143:70–83. https://doi.org/10.1016/j.carbpol.2016.02.002
42. Essabir H, Nekhlaoui S, Bensalah MO, et al (2017) Phosphogypsum waste used as reinforcing fillers in polypropylene based composites: structural, mechanical and thermal properties. J Polym Environ 25. https://doi.org/10.1007/s10924-016-0853-9
43. Tiouitchi G, Raji M, Mounkachi O, et al (2019) Black phosphorus-based polyvinylidene fluoride nanocomposites: synthesis, processing and characterization. Compos Part B Eng 175. https://doi.org/10.1016/j.compositesb.2019.107165
44. Mojarrad A, Jahani Y, Barikani M (2012) Influence of nanoclay on the rheological properties of polyamide 6/acrylonitrile butadiene styrene nanocomposites. J Appl Polym Sci 125:E571–E582. https://doi.org/10.1002/app.34092
45. Essabir H, Elkhaoulani A, Benmoussa K, Bouhfid R, Arrakhiz FZ, Qaiss A (2013) Dynamic mechanical thermal behavior analysis of doum fibers reinforced polypropylene composites. Mater Des 51:51–788. https://doi.org/10.1016/j.matdes.2013.04.092
46. Laaziz SA, Raji M, Hilali E, Essabir H, Rodrigue D, Bouhfid R, Qaiss A (2017) Bio-composites based on polylactic acid and argan nut shell: production and properties. Int J Biol Macromol 104:104–142. https://doi.org/10.1016/j.ijbiomac.2017.05.184
47. Araújo EM, Hage E, Carvalho AJF (2004) Thermal properties of nylon6/ABS polymer blends: compatibilizer effect. J Mater Sci 39:1173–1178. https://doi.org/10.1023/B:JMSC.0000013872.86575.36
48. Fornes TD, Yoon PJ, Keskkula H, Paul DR (2001) Nylon 6 nanocomposites: the effect of matrix molecular weight. Polymer (Guildf) 42:09929–09940. https://doi.org/10.1016/s0032-3861(01)00552-3
49. Raji M, Essassi E, Essabir H, et al (2019) Properties of nanocomposites based on different clays and polyamide 6/acrylonitrile butadiene styrene blends. In: Bio-based polymers and nanocomposites: preparation, processing, properties & performance. Springer International Publishing, pp 107–128
50. Bose S, Bhattacharyya AR, Kodgire PV, Misra A, Pötschke P (2007) Rheology, morphology, and crystallization behavior of melt-mixed blends of polyamide6 and acrylonitrile-butadiene-styrene: influence of reactive compatibilizer premixed with multiwall carbon nanotubes. J Appl Polym Sci 106:3394–3408. https://doi.org/10.1002/app.27018